



Coupled Analysis of Transient Aerodynamic Characteristics of the Coach under Crosswind in Different Situations

K. Sun^{1†}, Y. Yang^{1†}, Z. Gu², J. Liu¹, L. Zheng¹, H. Hu¹ and J. Gao¹

¹ State Key Laboratory of Advanced Design and Manufacturing for Vehicle Body, Hunan University, Changsha, 410082, Hunan, China

² Hunan University of Arts and Science, Changde, 415000, Hunan, China

†Corresponding Author Email: sk419@hnu.edu.cn

(Received April 11, 2020; accepted July 15, 2020)

ABSTRACT

The purpose of this work is to investigate transient aerodynamic characteristics of the coach under the crosswind in straight-line situations with different uniform speeds and uniform accelerations. The transient aerodynamics caused by different speed changes are analyzed using the real-time interaction between aerodynamic simulation and dynamic simulation. The target model is a simplified coach on a full scale. The SST (Menter) K-Omega Improved Delayed Detached Eddy Simulation and overset mesh technique are used to predict the transient aerodynamic loads. The accuracy of the turbulence model is verified by a wind tunnel experiment of the 1/7th scaled coach model. The present results show that the transient aerodynamic loads have different locations of maximum side force and the holding duration of yaw moment for different constant speeds. The speed becomes larger, and the position where the side force is maximum becomes farther away. The holding duration of the top yaw moment is larger simultaneously. Moreover, proper acceleration for low initial driving speed and crosswind of small influence range could build up stability. High speed driving in gust wind is not suggested for unskilled drivers.

Keyword: Coupled; Transient; MBD; CFD; Accelerate; DES; Overset; Crosswind.

NOMENCLATURE

A	the projected frontal area	v_c	crosswind velocity
C_D	drag coefficient	v_i	initial velocity
C_L	lift coefficient	v_r	relative velocity
C_S	side force coefficient	W	width of the coach
F_D	drag force	X	longitudinal distance
F_L	lift force	y^+	dimensionless wall distance
F_S	side force		
H	height of the coach	β	yaw angle
L	length of the coach	ρ	air density
L	wheelbase of the coach		
M_P	pitch moment		
M_R	roll moment		
M_Y	yaw moment		
Re	Reynolds number		
v	velocity in x-y plane		

Subscripts/Superscripts

c	initial
i	relative
r	crosswind

1. INTRODUCTION

In most cases, vehicle designer pays more attention to energy saving by reducing weight. Meanwhile, ground vehicles traveling on the highway at higher speeds are always affected by outside interference, such as the wind gusts and uneven roads. Many vehicle accidents caused by crosswinds were described in the study including overturning and course deviation accidents by Baker and Reynolds (1992). In their previous work, they developed a theoretical model based on the six equations of motion that enabled the wheel reactions and lateral and rotational displacements to be calculated for four different types of vehicles and allowed accident wind speeds to be calculated with consideration of inertial properties. High sided vehicles were confirmed more sensitive to crosswind by Baker (1987). Based on this result, it is very important to consider stability for coaches, which have large side area and high center of gravity.

At an early period, types of research about coaches' safety under crosswind have been done by wind tunnel tests using a quasi-steady method, which is a rough estimation of unsteady developments based on property interpolation during steady conditions by Wojciak (2012). With the help of the wind tunnel tests to measure aerodynamic loads at different yaw angles, the results implied that both side force and lift reached the maximum values when the wind direction was 30 degree in relation to the bus driving direction, which seriously affected the stability of the bus by Petzäll *et al.* (2005). Juhlin *et al.* investigated the bus crosswind directional stability by using the Multi-body dynamics (MBD) model combined with a generalized gust model and static wind tunnel measurements (Juhlin 2004; Juhlin and Eriksson, 2004; Juhlin 2008; Drugge and Juhlin, 2010). All the above aerodynamic forces were linearly fitted obtained from between minimum and maximum steady loads according to the change of yaw angle. However, the effects of transient gust were different from quasi-steady flow characteristics on both the structure and total pressure loss in the wake (Ryan and Dominy, 2000). Therefore, this approach cannot capture unsteady phenomena. The development of computational fluid dynamics (CFD) simulation made the realization of different turbulent scenarios and flow structure visualization easier. Hemida and Krajnović (2009) numerically studied the influence of three different windy gusts on a typical double-deck bus, and large fluctuations in transient aerodynamic coefficients were appeared due to unsteady behavior of the flow. Moreover, vehicles in motion are always accompanied by changes in body posture, resulting from outside disturbance or driver's operation, which also generates unsteady aerodynamic performances. As early as 1987, a comparison between dynamic and quasi-static force and moment data at nine yaw rates in the range 0.25 to 64deg/s was conducted at an open return wind tunnel and differences in aerodynamic loads were seen to be significant (Garry and Cooper, 1986). Furthermore, a series of investigations about the

influences of pitch motion on vehicle aerodynamic loads were performed by wind tunnel experiments or numerical simulations. Two different vertical height-adjustable devices in wind tunnel could realize quasi-static and dynamic angle change of attack of the model at which the phenomena of hysteresis and phase-shifting occurred in total pressure loss coefficients (Gilliéron *et al.* 2003). The hysteresis effects were also found in simulation (Krajnović *et al.* 2011; Gu *et al.* 2016). Nakashima *et al.* (2009) performed a numerical analysis of two kinds of simplified vehicle models with regard to vehicle pitch motion, comparing the result of the quasi-steady method with a non-stationary condition through the Arbitrary Lagrange-Euler (ALE) method to realize dynamic pitch motion.

In order to simulate the situation of vehicle driving on the road exposed to the unsteady flow condition, it is important to establish a real-time data feedback model between aerodynamic model and vehicle dynamic model. The fully-coupled 6 degrees of freedom (DOF) vehicle handling within MATLAB and CFD model allowed the vehicle body to roll, pitch and yaw in response to changing aerodynamic loads resulting from both vehicle postural changes and traversing the gust. Besides, the vehicle deviated laterally from its initial path. Hence real-time interaction between transient vehicle motion and aerodynamic loads was captured and assessed. What the work did show was little difference between a one-way and two-way coupled simulation for this car, but the quasi-steady and unsteady simulations had a big difference (Forbes *et al.* 2016). In contrary to the study of Forbes *et al.* the results show that a one-way coupled simulation over-predicts the aerodynamic loads and in turn the vehicle motion for the bus (Winkler *et al.* 2016). However, vehicle dynamic models used in the above two-way coupled methods were massively simplified about the detailed structural parameters. In our previous work (Li *et al.* 2018; Liu *et al.* 2019), the more accurate dynamic model based on the commercial software ADAMS/Car was established. And the real-time exchange of aerodynamic loads from the CFD model and motion data from the MBD model was done automatically by the two codes with some user-defined functions. The result indicated that the vehicle would be more unstable owing to the low road adhesion and the crosswind (Li *et al.* 2018). Because the one-way coupling method cannot fully capture the unsteady flow characteristics in the overtaking process, differences of the aerodynamic loads and the vehicle dynamic response between one-way and two-way coupled approaches were visible in different transverse spacings (Liu *et al.* 2019).

In this paper, the analysis of transient aerodynamic characteristics of the coach was focused on different driving speeds including four kinds of constant velocities and three different accelerations using the two-way coupling method. The SST (Menter) K-Omega Improved Delayed Detached Eddy Simulation and overset mesh technique in the CFD simulation were used to predict the transient

24.12m/s respectively, corresponding to the end speed driving at different accelerations after the distance of 5.5L without the influence of crosswind. In addition, a driving speed of 20m/s is used as a reference.

The relative velocity v_r represents the velocity of the coach relative to the flow in x-y plane, which is defined as

$$v_r = \sqrt{v^2 + v_c^2} \quad (1)$$

The yaw angle β indicates the angle between the coach's moving orientation and negative direction of the x-axis of the overall reference frame, which is

$$\beta = \arctan(v_c / v) \quad (2)$$

The crosswind profile is selected the same as the wind tunnel experiment conducted by [Chadwick *et al.* \(2001\)](#). As shown in Fig. 3, the ramp-up and ramp-down curves are modeled using a cosine function ([Favre and Efraimsson, 2011](#)). When the coach with a speed of 20m/s travels through a crosswind zone with a wind speed of 12m/s, a maximum relative yaw angle of 30deg is simulated corresponding to the dangerous angle ([Petzäll *et al.* 2005](#)). Non-dimensional length X/L is the ratio of the distance of forwarding movement to the length of the body after the crosswind attacks the coach's front end.

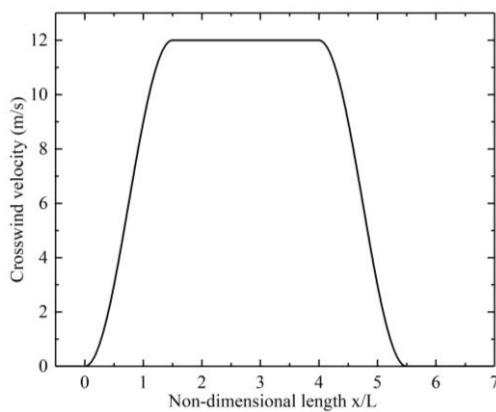


Fig. 3. Accelerating driving situation.

2.2 Numerical Simulation

2.2.1 Aerodynamics

The Newtonian fluid is assumed, which is also viscous and unsteady. The Mach number is quite small when the vehicle moves at a velocity less than 120km/h, so the external flow field of the coach belongs to three-dimensional(3D) incompressible flow condition ([Yuan *et al.* 2018](#)). The typical Reynolds number of the flow cases with respect to the vehicle length and base running velocity of 20m/s in the x-direction is 1.567×10^7 , which is independent results ([Solmaz and İcingür, 2015](#)). To accurately simulate the flow structure around the

coach, it is necessary to use a hybrid method turbulence model. Here, the Detached Eddy Simulation (DES) approach, as a hybrid model of RANS and LES, superior to predict aerodynamic characteristics and wake flows for high Reynolds number, massively separated flows, is used and the improved delayed Detached Eddy Simulation model eliminates the suboptimal performance of DES ([Li *et al.* 2020](#)). Moreover, the chosen underlying RANS model is the Spalart-Allmaras turbulence model ([Gritskevich *et al.* 2012](#)). And the governing equations of SST- IDDES and parameter settings refer to our previous research ([Liu *et al.* 2019](#)).

The computational domain ($x=20L, y=15W, z=5H$) of all aerodynamic simulations is in a rectangular region that is divided into 19.4 million unstructured hexahedral trimmed grids. [Favre and Efraimsson \(2011\)](#) concluded that hexahedral mesh was better to capture turbulent structure in the wake. The overset region including refining meshes is composed of 12.6 million cells and the refining method will be presented in Fig. 4. The smallest element size on the coach surface is 8mm, whilst 8 prism layers to a combined wall-normal distance of 8.25mm with stretching of 1.2 to ensure a $y^+ < 20$ on most vehicle surfaces. The initial placement of the coach is 6L from its front end to the background boundary, combined with different distances for different velocities to the crosswind beginning, which can result in one-half second initialization period, before the crosswind attacks the coach. Considering the lateral distance caused by crosswind and fluid developing unaffected by inlet backflow, 3W from the side inlet and 5H from the background ceiling are sufficient ([Yuan *et al.* 2018](#)). For all simulations, as shown in Fig. 4, two inlets and outlets are used, in which the front is a velocity inlet of zero speed but the right is with a fixed crosswind band ([Forbes *et al.* 2016](#)). No-slip wall condition is on the top and bottom boundaries.

The overset technique is used to realize the movement of the coach as a result of the driving operation and crosswind. Here, the overset regions include the wheels and the body respectively in the same as [Forbes *et al.* \(2016\)](#). In view of computing resources and the sensitivity to the grid size of the overset method, the horizontal motions of four wheels are only taken into account, which yields 3DOF for each wheel. The coach body can realize the motion of 6DOF considering suspension and crosswind effects. Both regions have a common background region containing multiple mesh refinement zones in running route to guarantee overset mesh interpolation, similar to [Favre and Efraimsson \(2011\)](#). At the same time, both overlap regions move with coach motion relative to the background region. In order to avoid the interpolation error of the overset method, the refining region elements of the coach driving line of the background are the same as the surrounding mesh size of the outside surface of three regions, which are 200mm except the junction of wheels and ground. Here, the overset-background interface uses the least square interpolation ([De Luca *et al.* 2016](#)). The

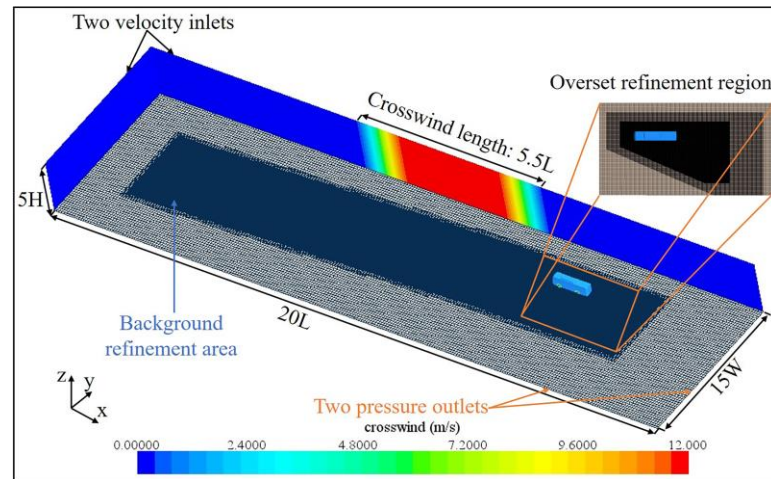


Fig. 4. Computational domain and boundary condition.

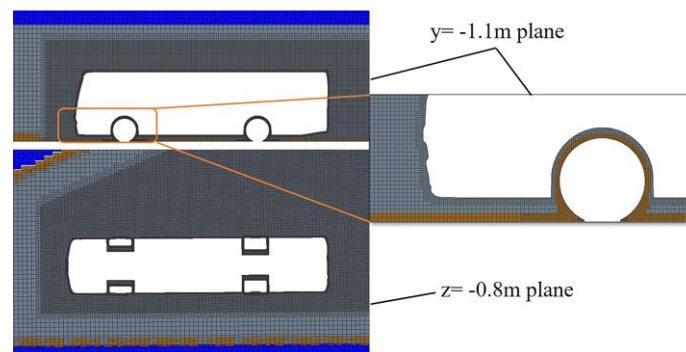


Fig. 5. Overset grid.

overset mesh regions are shown in Fig. 5, including a coach-body region and a coach-wheels region.

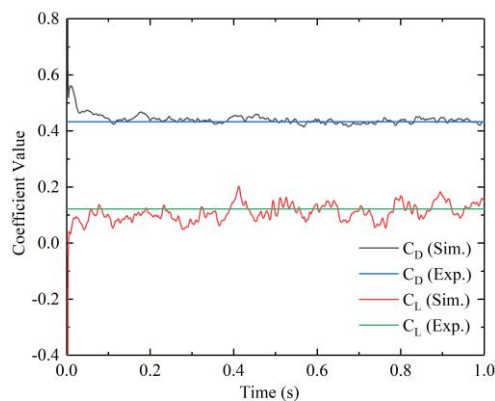


Fig. 6. Drag and Lift coefficient convergence during initialization period.

The time step is set as 1×10^{-4} s to make sure the Convective Courant Number below one in most of the regions and a second-order time discretization scheme is adopted to limit the numerical dissipation of flow combined with a hybrid second-order bounded central-differencing scheme used in space. The reference density is 1.2039 kg/m^3 , and the

turbulence intensity is 0.13%, consistent with the wind tunnel test (Yuan *et al.* 2018). Figure 6 indicates that the aerodynamic coefficient has converged after 0.5s. The lift and drag coefficients fluctuate around the experimental value. Therefore, 0.5 seconds of initialization is reasonable.

The CFD simulations were performed in CD-Adapco's Star-CCM+ v10.04.009 and run on an H3C power server at the Hunan Institute of Science and Technology with eight nodes, 12 processors, and 128 GB memory for each node. Firstly, all simulations run for three seconds when the coach was stationary to ensure full development of turbulence. Then a total physical time of five seconds with the coach moving was conducted, including one-half second independent initialization and the remaining time for the coupled simulation. It took about 75 hours for every case.

2.2.2 Whole Vehicle Multi-Body Dynamics (MBD)

The commercial software package MSC.ADAMS/Car is used to construct the vehicle MBD model from real vehicle's testing parameters and realizes the vehicle's handling behaviors, which takes full advantage of sparse matrix processing techniques to solve mechanical systems. Governing equations of multi-body dynamics can refer to our previous work (Li *et al.* 2018; Liu *et al.* 2019)

Table 1 Vehicle parameters for the multi-body dynamic model

Parameters	Values	Parameters	Values
Totally degree of freedom	80	Number of moving parts	59
Number of constraints	69	The front end to CG	4.744 [m]
Whole vehicle quality	11900 [kg]	Height of CG	0.972 [m]
Front wheelbase to CG	2.743 [m]	Rear wheelbase to CG	3.257 [m]
Front wheel tread	2.134 [m]	Rear wheel tread	1.884 [m]
Rolling moment of inertia	3336.4[kg·m ²]	Pitching moment of inertia	54216.3 [kg·m ²]
Yawing moment of inertia	53752.6 [kg·m ²]	Stiffness of the front suspension	131166.7[N/m]
Stiffness of the rear suspension	145821.4 [N/m]	Damping of suspension	15153.8[N·s/m]
Cornering stiffness of tyre	977.2 [N/deg]	vehicle sprung mass	8134 [kg]

The virtual prototype model of the coach is constructed based on the parameters from the existing coach in Table. 1, which includes rigid body system, power system, transmission assembly system, front suspension system, steering system, back suspension system, tire system, a general aerodynamic force element and so on shown in Fig. 7.

As our previous studies mentioned, the aerodynamic loads from real-time CFD data are applied to the CG of the rigid body (center of the yellow sphere in Fig.7) by general force element (Li *et al.* 2018; Liu *et al.* 2019), which is not the CG of the whole coach seen in Table. 1. To avoid additional interference like virtual road roughness and unstable beginning running of the MBD software, the 2D-flat road model is used with 1.0 as the adhesion coefficient and the MBD model runs in a straight line for 0.5s before real-time data exchange.

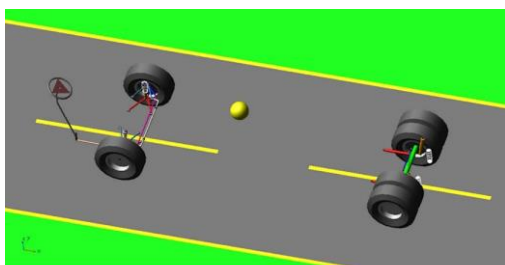


Fig. 7. Full vehicle ADAMS/Car Model with Road.

The time step of the MBD simulation is 1×10^{-4} s corresponding to the CFD simulation, in which the data of aerodynamic loads and motion parameters is

exchanged respectively by the java API of Star-CCM+ and the user subroutines of ADAMS/Car. Event Builder function of ADAMS/Car is for setting different driving situations by defining the Mini-Maneuver parameters. In this paper, driver model is not considered to show the effect of transient aerodynamics on the coach obviously.

3. COMPUTATIONAL VALIDATION

3.1 Wind Tunnel Experiment

To validate the accuracy of the selected turbulence model to calculate aerodynamic loads, a wind tunnel test of the 1/7th scaled coach model was carried out in the closed-circuit subsonic reduced-scale wind tunnel of Hunan University. The projected frontal area of the coach model is 0.1678595m². The cross-sectional area of the wind tunnel is 3×2.5m², which results in a blockage ration of about 2.24% for the frontal area of the scaled model. And the maximum speed is 58m/s. The average turbulence intensity of upstream is about 0.13% (Yuan *et al.* 2018). The pumping system was used to eliminate the boundary layer in front of the coach model (Wang *et al.* 2014).

The model was fixed at the center of the turntable and the aerodynamic force was measured by a six-component balance, as shown in Fig.8. The non-dimensional coefficients are defined as follows:

$$C_D = \frac{F_D}{\frac{1}{2} \rho v^2 A}, C_L = \frac{F_L}{\frac{1}{2} \rho v^2 A}, C_S = \frac{F_S}{\frac{1}{2} \rho v^2 A} \quad (3)$$

Where F_D , F_S and F_L represent the forces correspondingly, ρ is the air density, A represents the projected frontal area of the coach and v indicates the

forward velocity of the coach. All the aerodynamic coefficients are normalized with $\rho = 1.2039\text{kg/m}^3$, $v = 30\text{m/s}$ and $A = 0.1678595\text{m}^2$.



a



b

Fig. 8. Wind tunnel test (a) model location (b) external six-component balance.

3.1.1 Grid Independence Verification

For all simulations, the coordinate was consistent with the test and four refining sizes of cell generation had been studied to exclude the influence of grids on calculations. The computational domain and boundary conditions were the same as the investigation by Wang *et al.* (2014). It is very expensive to simulate all cases for validating the grid independence with different yaw angles. So 0deg yaw angle was only considered and the aerodynamic coefficient C_D and C_L were the averages of last 1000 steps in a 2s total sampling time. Similarly, the measured values of the wind tunnel test were the average value after the forces were stable.

The results were compared with the test in table. 2. The stable value of the aerodynamic drag coefficient was about 8.1% smaller than the experimental value, which was reasonable for this turbulent model (Delassaux *et al.* 2020). The counterpart for C_L was 8.3%, but less than 10%. Therefore, the refining method of case 3 was used in other simulations.

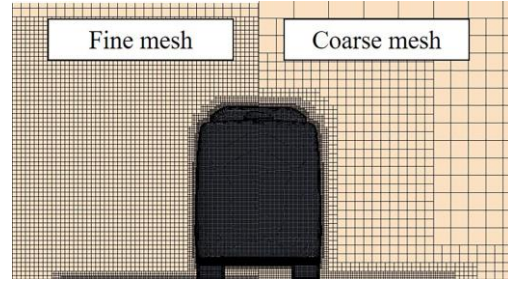


Fig. 9. Grid generating condition.

Table 2 Comparison of different grid size simulation with test

Case	No. of cells $\times 10^6$	C_D	C_L
Case1	5.43	0.444	0.151
Case2	7.63	0.437	0.148
Case3	8.95	0.433	0.145
Case4	10.53	0.433	0.144
Experiment	-	0.471	0.157

3.1.2 Turbulent Model Verification

Here, three aerodynamic loads including the drag in the streamwise direction, the side force in the lateral direction and the lift in the upward vertical direction were measured in wind tunnel test and CFD simulation. On the one hand, the coach was subjected to a steady side wind with a 30m/s speed along the positive x-axis and yaw angles of the coach with respect to x-axis direction was 0deg, 3deg, 6deg, 9deg, 12deg, 15deg. On the other hand, the aerodynamic data of the wind tunnel experiment was the average of 20 sets of data after the wind speed was stabilized to avoid random errors.

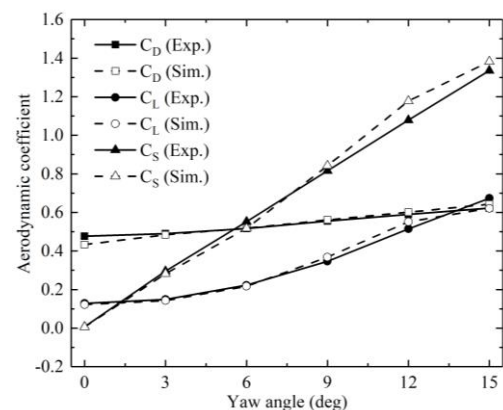


Fig. 10. Aerodynamic coefficient of measurement and calculation for the yaw angle range.

Figure. 10 showed the time-averaged values of the aerodynamic coefficients obtained from simulations and tests. At this stage, the changing trend of aerodynamic coefficients with the yaw angle was the same as the experiment. The differences of all aerodynamic coefficients between test and simulation were less than 10%. Therefore, the selected method was reliable for the present paper to predict the aerodynamic change trend.

3.2 Demonstrating the Robustness of the Multi-Body Dynamic Model

Due to the difficulties to control the road test reproducibility and eliminate other non-crosswind interference factors, a parameter study was conducted to show the ability of the MBD model ability to capture the expected motions caused by crosswind. Similar to previous researches (Li *et al.* 2018; Liu *et al.* 2019), other aerodynamic loads apart from drag were exerted on the different locations of the coach body at arbitrary time-varying value presented in Fig. 11. The aerodynamic loads were applied using a GFORCE element after 0.5 seconds of running initialization. In addition to acting on the CG, the location of this action center was set moving in the vertical and longitudinal directions with upward (UD), downward (DD), forward (FD) or backward (BD) directions of 0.5m and 1m relative to the CG.

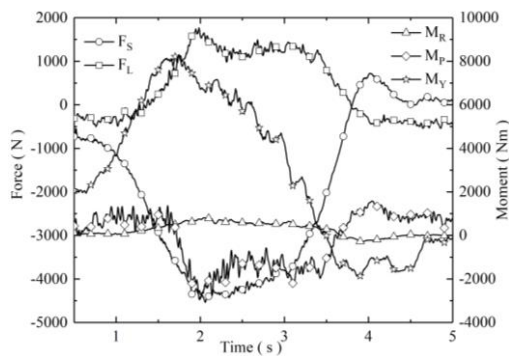


Fig. 11. Aerodynamic loads applied to the body.

As shown in Fig. 12, the lateral displacement became larger when the loads acting position was located in front of and above the CG and smaller on the counterpart. On the other hand, the roll angle also showed the opposite trend for the opposite position movement direction. Different positions caused the new moments different from the origin and different body motions were captured. It indicated that the MBD model had a good response to changes in aerodynamic loads. Therefore, the MBD model is reliable to capture the expected changes of the vehicle motion.

4. RESULTS

In this section, the results from the fully coupled

numerical simulations of a coach passing through a transient crosswind with different velocities and accelerations are presented and discussed. All aerodynamic loads adopt the aerodynamic coordinate system SAE J1594 (SAE Surface Vehicle Recommended Practice, 2010). In all figures, 20_con, 21_con, 22_con and 24_con represent the straight driving situations of the coach with the constant speed of 20m/s, 21.46m/s, 22.83m/s and 24.12m/s respectively. 04_acc, 08_acc and 12_acc mean that the coach is driven in a straight line with uniform positive acceleration of 0.4m/s², 0.8m/s² and 1.2m/s².

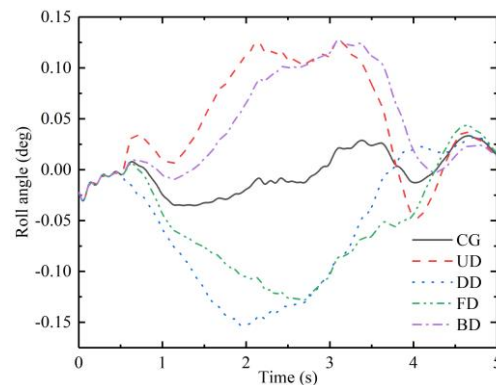
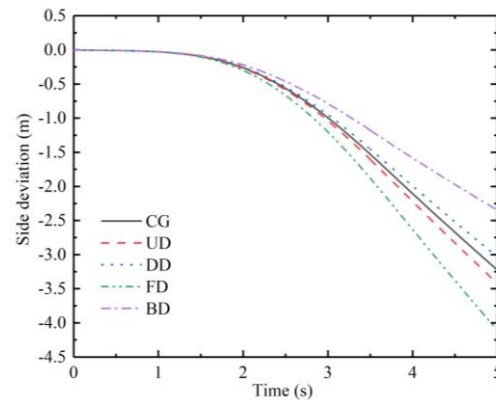


Fig. 12. Results of different acting position (a) side deviation in longitudinal direction (b) roll angle in the vertical direction.

In Fig. 13, the opposite orientation of crosswind direction was used to facilitate the analysis of changes in lateral forces. It could be seen that the driving distance became greater when the coach driving speed increased, where the side force reached its maximum. For example, the displacement of 2.649L was needed for 20_con, corresponding to the 1.149 body length in the area with the highest crosswind wind speed and 1.537deg of the yaw angle. While the displacement of 2.974L was needed for 24_con, corresponding to the 1.474 body length in the area with the highest crosswind wind speed similar to the result (Petzäll *et al.* 2005)

and 1.814deg of the yaw angle. When driving at a high speed, even if the yaw angle changed slightly, the impact of the vehicle driving on the lateral force was relatively large.

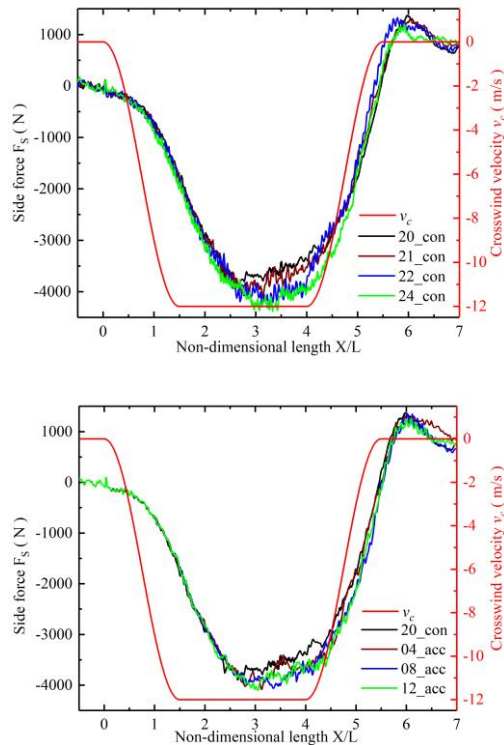


Fig. 13. Side force for different driving cases.

The greater the speed for constant velocity, the longer the driving distance at the maximum yaw moment shown in Fig. 14(a), while the greater the acceleration, the smaller the holding distance of the maximum yaw moment for accelerating cases presented in Fig. 14(b). The position of the maximum yaw moment was located at the driving distance of 2L for the accelerating condition, where the distance of the coach nose into the crosswind stability zone was 0.5L. However, the maximum yaw moment was reached at one and a half bus body length further into the crosswind from studies of Juhlin (Juhlin, 2004; Juhlin and Eriksson, 2004; Juhlin, 2008; Drugge and Juhlin, 2010) and Chadwick's study showed a maximum yaw moment at one body length into the gust. The differences were derived from the consideration of the real-time effects of aerodynamic loads and vehicle motions in this paper, which was more in line with actual road driving.

For coach dynamic response at the horizontal, the higher speed caused bigger crests and troughs shown in Fig. 17(a). For example, the maximum yaw rate for 24_con was 33% above the maximum of yaw rate for 20_con and the minimum for 24_con was 2 times the minimum for 20_con. In Fig. 17(b), there was only a small difference in the yaw rate before reaching the minimum value, and even the

acceleration made the yaw rate smaller for a long time. As the speed difference increased, the gap between the minimum values became larger. The biggest gap between the minimums was 0.36deg/s. When the rear end of the coach was driven out of the side wind zone ($X/L=6.5$), the smallest accumulated deviation from the original path was 2.168m from 24_con described in Table. 3. At the same time, the top yaw angle due to the crosswind was also minimal. However, due to the relatively large peak of side force and yaw moment, the effect on the driver's operation was also unfavorable. For these accelerating cases, the maximum yaw angle was no big difference and the deviation with $X/L=6.5$ was similar. Therefore, proper acceleration at low initial speed is beneficial.

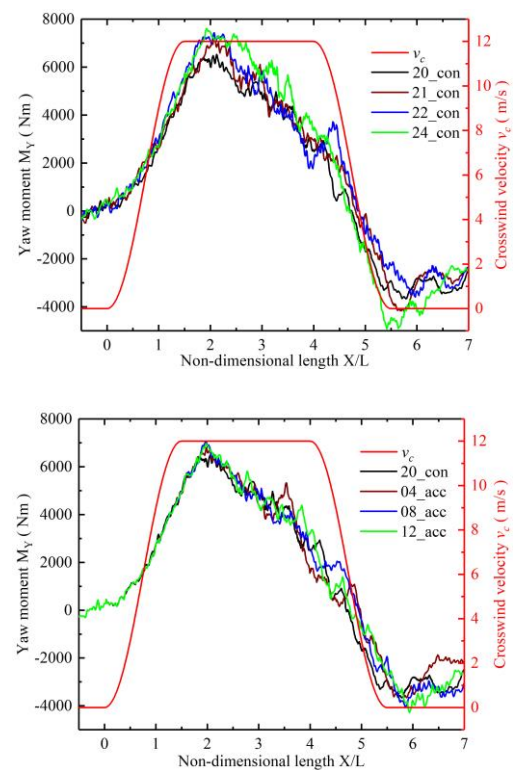


Fig. 14. Yaw moment for different driving cases.

Moreover, the roll moment was presented in Fig. 15 and the maximum roll moment reached when the vehicle was completely immersed in the maximum crosswind area for all cases. High speed reduced the duration of roll moment peaks contrary to the tendency of yaw moment changing for constant speed situations, while both of them increased peaks in Fig. 15(a). The presence of acceleration affected the roll moment peak, which became irregular with speed indicated by Fig. 15(b). The value of the roll angle at different positions was presented in Fig. 16, which was relatively gentle near the minimum for large acceleration. What's more, large speed caused large fluctuations of roll angle. For 24_con, angle

fluctuation value reached 0.16deg, which didn't affect stability.

relative flow velocity around the body caused more fluid separation phenomena.

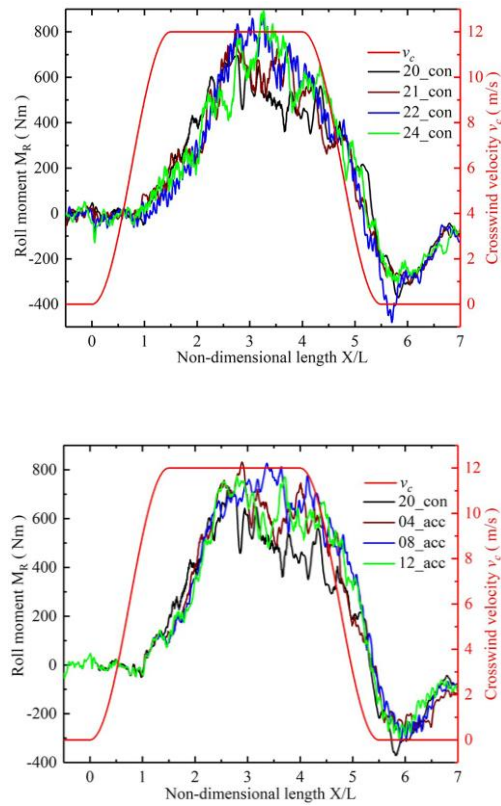


Fig. 15. Roll moment for different driving cases.

Table 3 The lateral deviation(X/L=6.5) and maximum yaw angle for different cases

Cases	Deviation(m)	Angle(deg)	X/L
20_con	2.370	3.279	5.516
21_con	2.314	3.286	5.5
22_con	2.218	3.204	5.503
24_con	2.168	3.154	5.352
04_acc	2.352	3.324	5.612
08_acc	2.349	3.371	5.647
12_acc	2.349	3.365	5.678

It was obvious that the influence of the increase in constant speed on the frequency of aerodynamic loads fluctuations was higher than the driving situations caused by these accelerations. A large

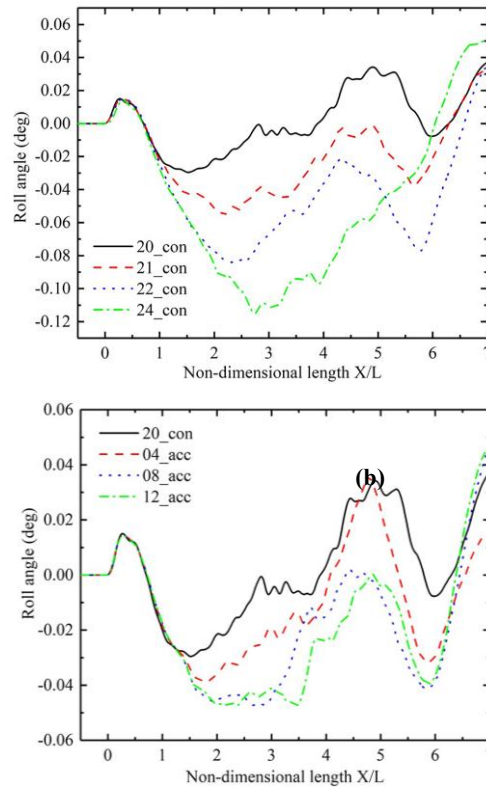


Fig. 16. Roll angle for different driving cases.

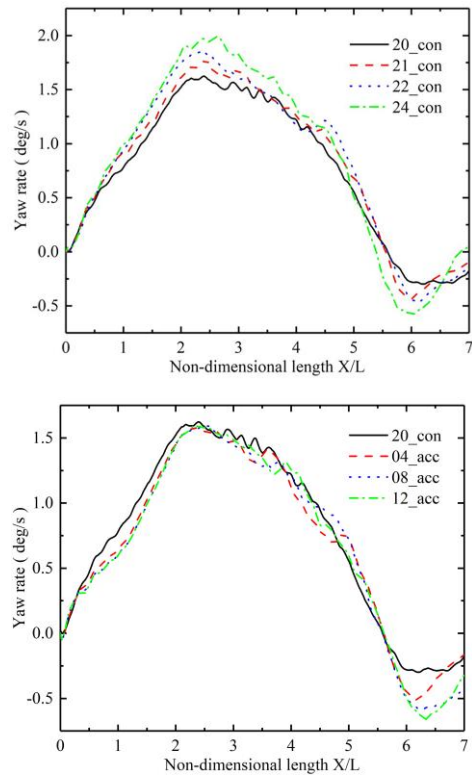


Fig. 17. Yaw rate for different driving cases.

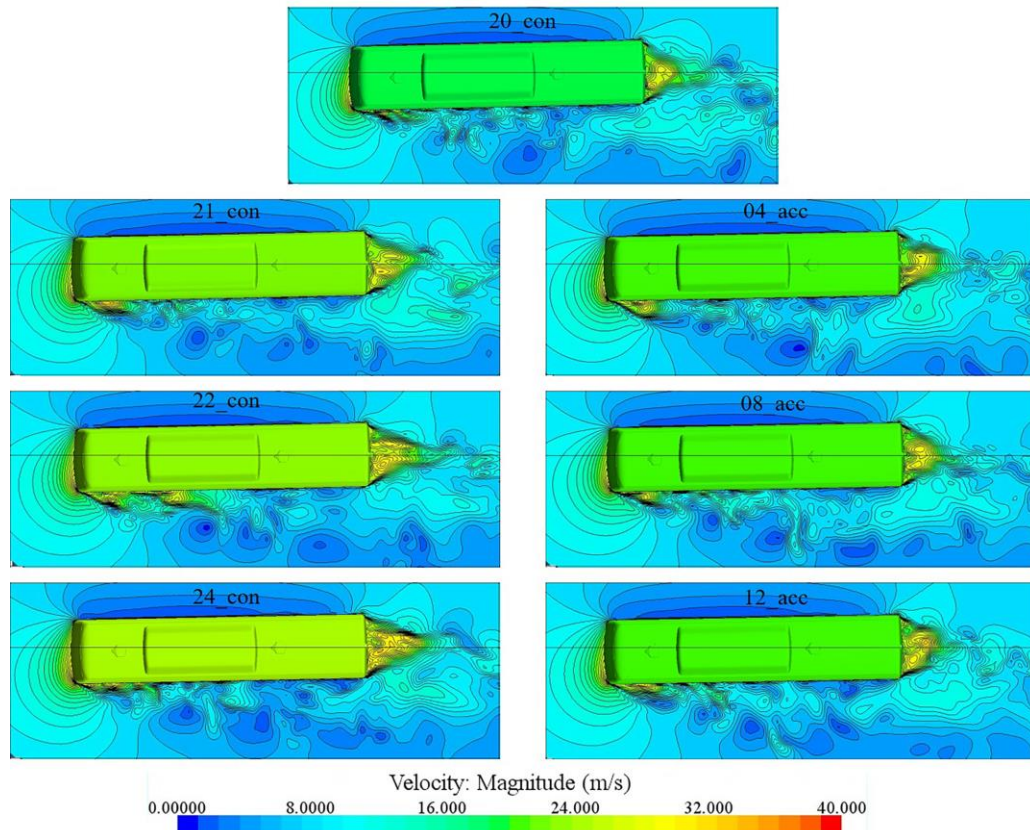


Fig. 18. Snapshots of the flow velocity magnitude ($X/L = 3.25$ and $z = 0$).

In Fig. 18, the flow condition of the windward and leeward side of the coach for different cases was depicted. Because of the crosswind and the movement of the coach body, large separation zones produced different forms of flow separation at the leeward side and the rear end resulting in different low-pressure distributions. Combined with the high-pressure area at the upwind side, it generated different fluctuating aerodynamic loads.

5. CONCLUSION

Common driving conditions on the road were realized in this study, which applied the real-time interaction between the CFD software and the MBD software. Using Detached Eddy Simulation (DES) combined with the overlap mesh technique was to compute aerodynamic loads caused by crosswind and achieved the coach motion from ADAMS/Car. The aim of this work was to assess the effect of different speeds on transient aerodynamic loads from constant and accelerating driving conditions.

The transient response from the wind tunnel is originated from the wind gust and it is difficult to measure the transient aerodynamic loads generated by the interaction of body's transient motion and aerodynamics. There is an important difference between wind tunnel tests and real road conditions. Through the research in this article, the following conclusions can be drawn. On the one hand, the

results indicate that different constant velocities obviously change the position of maximum side force and the holding duration of top yaw moment. The speed becomes larger, and the position where the side force is maximum became farther away. The holding duration of the top yaw moment is larger simultaneously. If the driver overreacts to the crosswind, a slight oversteering operation will result in large transient aerodynamic loads. Although it has a small amount of the lateral path deviation, it produces an excessive yaw rate, which seriously affects the directional stability of the coach. On the other hand, proper acceleration for low initial driving speed and the crosswind of small influence range can weaken instability. For all simulations, the transient roll motion is too small to be ignored for this wind gust condition. An accelerating event with bigger acceleration, may bring out more noticeable variations and hence is the next application of this simulation method.

ACKNOWLEDGEMENTS

The work was supported by National Natural Science Foundation of China (Grant No. 51875186); Key Research and Development Program of Hunan Province (2017GK2203), Independent Subject of State Key Laboratory of China (Grant No.734215002); and Major Science and Technology Projects of Changde (CD201701 The development

and application of lightweight and low-air-resistance integral body of electric bus)

REFERENCE

- Baker, C. J. (1987). Measures to control vehicle movement at exposed sites during windy periods. *Journal of Wind Engineering and Industrial Aerodynamics* 25(2), 151-161.
- Baker, C. J. and S. Reynolds (1992). Wind-induced accidents of road vehicles. *Accident Analysis & Prevention* 24(6), 559-575.
- Chadwick, A., K. Garry and J. Howell (2001). Transient aerodynamic characteristics of simple vehicle shapes by the measurement of surface pressures. *SAE*, 2001-01-0876.
- De Luca, F., S. Mancini, S. Miranda and C. Pensa (2016). An extended verification and validation study of CFD simulations for planing hulls. *Journal of Ship Research* 60(2), 101-118.
- Delassaux, F., V. Herbert, I. Mortazavi and C. Ribes (2020). Numerical Investigation of the Flow Around a Simplified Ground Vehicles Using Hybrid RANS/LES Method, *Progress in Hybrid RANS-LES Modelling*. Springer, Cham, 357-365.
- Drugge, L. and M. Juhlin (2010). Aerodynamic loads on buses due to crosswind gusts: extended analysis. *Vehicle system dynamics* 48(S1), 287-297.
- Favre, T. and G. Efraimsson (2011). An assessment of detached-eddy simulations of unsteady crosswind aerodynamics of road vehicles. *Flow, Turbulence and Combustion* 87(1), 133-163.
- Forbes, D. C., G. J. Page, M. A. Passmore and A. P. Gaylard (2016). A Fully Coupled, 6 Degree of-Freedom, Aerodynamic and Vehicle Handling Crosswind Simulation using the DrivAer Model. *SAE International Journal of Passenger Cars-Mechanical Systems*.
- Garry, K. P. and K. R. Cooper (1986). Comparison of quasi-static and dynamic wind tunnel measurements on simplified tractor-trailer models. *Journal of Wind Engineering and Industrial Aerodynamics* 22(2-3), 185-194.
- Gilliéron, P., F. Chometon and J. Laurent (2003). Analysis of hysteresis and phase shifting phenomena in unsteady three-dimensional wakes. *Experiments in fluids* 35(2), 117-129.
- Gritskevich, M. S., A. V. Garbaruk and J. Schützeand V. Menter (2012). Development of DDES and IDDES formulations for the $k-\omega$ shear stress transport model. *Flow, turbulence and combustion* 88(3), 431-449.
- Gu, Z. Q., T. M. Huang and Z. Chen Y. Q. Zong and W. Zeng (2016). Large Eddy Simulation of the Flow-Field around Road Vehicle Subjected to Pitching Motion. *Journal of Applied Fluid Mechanics* 9(6).
- Hemida, H. and S. Krajnović (2009). Transient simulation of the aerodynamic response of a double-deck bus in gusty winds. *Journal of Fluids Engineering* 131(3).
- Juhlin, M. (2004). Directional stability of buses under influence of crosswind gusts. *Vehicle System Dynamics* 41, 93-102.
- Juhlin, M. (2008). Aerodynamic loads on buses due to crosswind gusts—on-road measurements. *Vehicle System Dynamics* 46(S1), 827-835.
- Juhlin, M. and P. Eriksson (2004). A vehicle parameter study on crosswind sensitivity of buses. *SAE Technical Paper*.
- Krajnović, S., A. Bengtsson and B. Basara (2011). Large eddy simulation investigation of the hysteresis effects in the flow around an oscillating ground vehicle. *Journal of fluids engineering* 133(12).
- Li, M., B. Liu, T. H. Liu and Z. J. Guo (2020). Improved Delayed Detached Eddy Simulation of the Slipstream and Trackside Pressure of Trains with Different Horizontal Profiles, *Journal of Applied Fluid Mechanics* 13(2), 457-468.
- Li, S., Z. Gu, T. Huang, Z. Chen and J. Liu (2018). Coupled analysis of vehicle stability in crosswind on low adhesion road. *International Journal of Numerical Methods for Heat and Fluid Flow* 28(8), 1956-1972.
- Liu, J., Z. Gu, T. Huang S. Li, L. Zheng and K. Sun (2019). Coupled analysis of the unsteady aerodynamics and multi-body dynamics of a small car overtaking a coach. *Proceedings of the Institution of Mechanical Engineers, Part D: Journal of Automobile Engineering* 233(14), 3684-3699.
- Nakashima, T., M. Tsubokura, T. Nouzawa and M. Ichimiya (2009). Flow structures above the trunk deck of sedan-type vehicles and their influence on high-speed vehicle stability 2nd report: Numerical investigation on simplified vehicle models using Large-Eddy Simulation. *SAE International Journal of Passenger Cars-Mechanical Systems* 2(2009-01-0006), 157-167.
- Petzäll, J., P. Albertsson, T. Falkmer and U. Björnstig (2005). Wind forces and aerodynamics: contributing factors to compromise bus and coach safety. *International Journal of Crashworthiness* 10(5), 435-444.
- Ryan, A. and R. G. Dominy (2000). Wake Surveys Behind a Passenger Car Subjected to a Transient Cross-Wind Gust, *SAE Paper No. 2000-01-0874*.
- SAE Surface Vehicle Recommended Practice* (2010). Vehicle Aerodynamics Terminology, SAE Standard J1594, Rev. Jul. 2010.

- Solmaz, H. and Y. İcingür (2015). Drag Coefficient Determination of a Bus Model Using Reynolds Number Independence. *International Journal of Automotive Engineering and Technologies* 4(3), 146-151.
- Wang, Y., Z. Gu, S. Wang, Y. Deng and X. Yang" (2014). Numerical and Experimental Investigations on the Aerodynamic Characteristic of Three Typical Passenger Vehicles. *Journal of Applied Fluid Mechanics* 7(4),6859-6671.
- Winkler, N., L. Drugge, A. S. Trigell and G. Efraimsson (2016). Coupling aerodynamics to vehicle dynamics in transient crosswinds including a driver model. *Computers & Fluids* 138, 26-34
- Wojciak, J (2012). *Quantitative analysis of vehicle aerodynamics during crosswind gusts*, PhD Thesis, Technische Universität München.
- Yuan, Z., Z. Gu, Y. Wang and X. Huang (2018). Numerical investigation for the influence of the car underbody on aerodynamic force and flow structure evolution in crosswind. *Advances in Mechanical Engineering* 10(10), 1687814018797506.